**Working Group I Contribution to the**
**Intergovernmental Panel on Climate Change**
**Fourth Assessment Report**

**Climate Change 2007: The Physical Science Basis**

---

# Technical Summary

---

**Coordinating Lead Authors:** Susan Solomon, Dahe Qin, Martin Manning

**Lead Authors:** Nathaniel Bindoff, Zhenlin Chen, Amnat Chidthaisong, Jonathan Gregory, Gabriele Hegerl, Martin Heimann, Bruce Hewiston, Fortunat Joos, Jean Jouzel, Vladimir Kattsov, Ulrike Lohmann, Taroh Matsuno, Mario Molina, Neville Nicholls, Jonathan Overpeck, Graciela Raga, Venkatachalam Ramaswamy, Jiawen Ren, Matilde Rusticucci, Richard Somerville, Thomas Stocker, Ronald Stouffer, Penny Whetton, Richard Wood, David Wratt

**Contributing Authors:** Guy Brasseur, Jens Hesselbjerg Christensen, Kenneth Denman, Piers Forster, Eystein Jansen, Philip Jones, Hervé Le Treut, Peter Lemke, Gerald Meehl, David Randall, Kevin Trenberth, Jurgen Willebrand, Francis Zwiers

**Review Editors:** Kansri Boonpragob, Filippo Giorgi, Bubu Pateh Jallow

**Date of Draft:** 31 March 2006

**Figures**

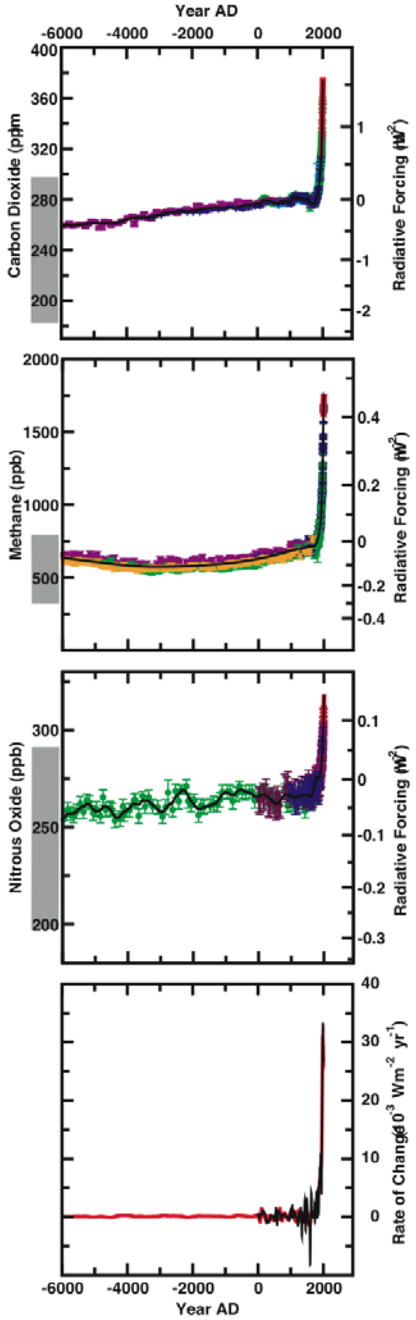


**Figure TS-1.** Atmospheric concentrations of carbon dioxide ($CO_2$), methane ($CH_4$), nitrous oxide ($N_2O$), and the rate of change in their combined radiative forcing. In the upper three panels, symbols denote measurements from ice cores or atmospheric samples and smoothed values are denoted by a solid line. Grey bars show the ranges associated with changes from ice ages to intervening warm periods over the past 650,000 years. Estimated radiative forcings due to changes since 1750 are indicated on the right hand side. The rate of change in total radiative forcing from all three gases is shown in the bottom panel with different amounts of smoothing corresponding to the averaging occurring in low accumulation (red) and high accumulation (black) ice cores. [Figure 6.4]

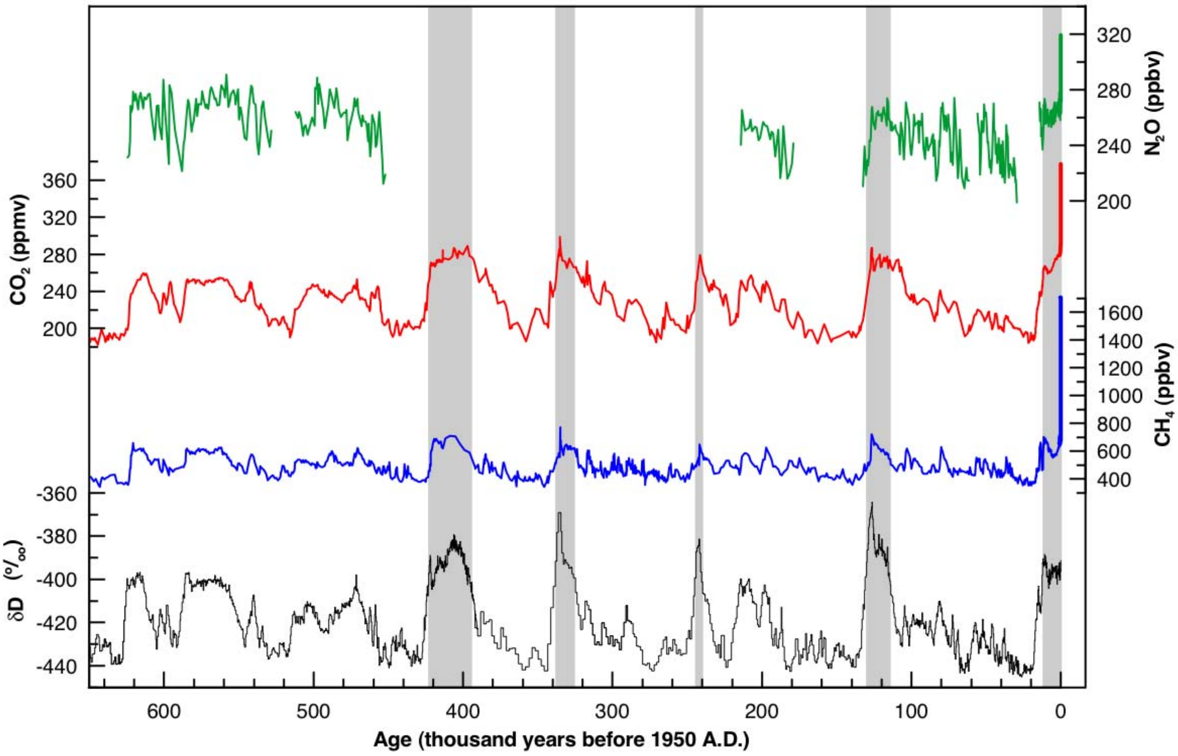


**Figure TS-2.** Variations of deuterium (δD) in Antarctic ice, which is a proxy for local temperature, and the atmospheric concentrations of the greenhouse gases carbon dioxide ($CO_2$), methane ($CH_4$), nitrous oxide ($N_2O$) derived from air trapped within ice cores from Antarctica and from recent atmospheric measurements. The shading indicates the last interglacial warm periods. [Figure 6.3]

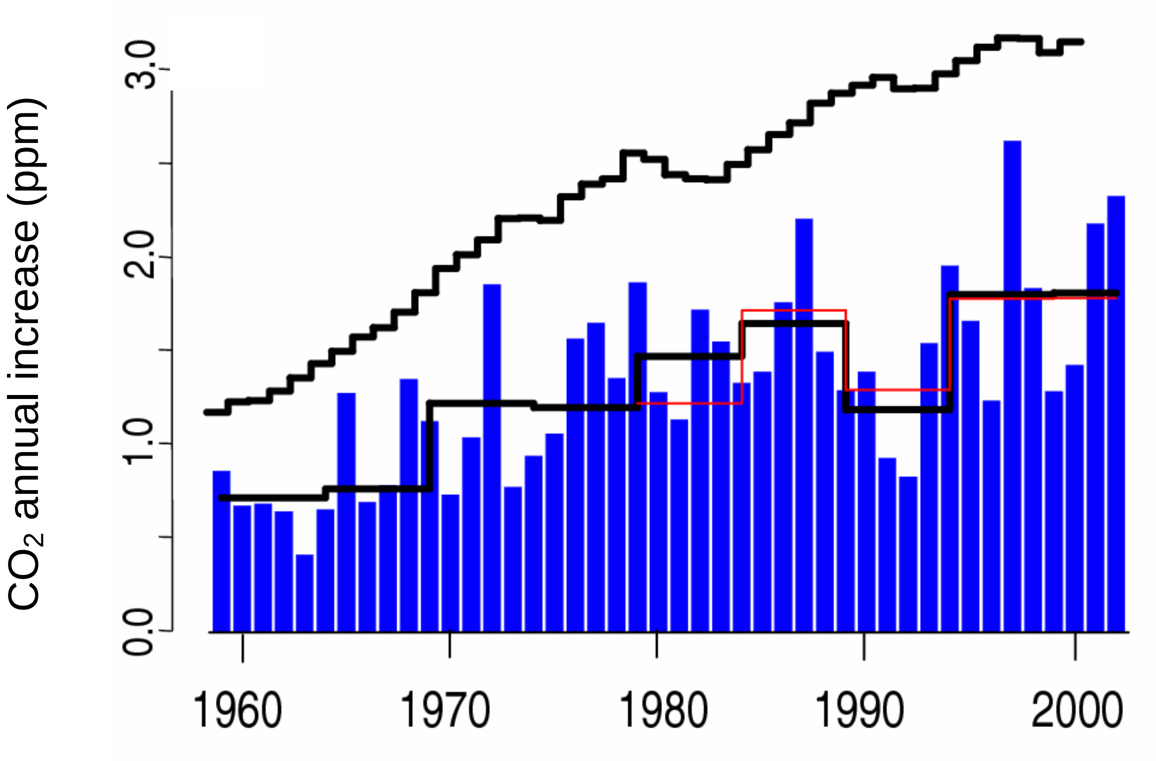


**Figure TS.3.** Atmospheric $CO_2$ increases: Blue columns show observed annual changes in global atmospheric $CO_2$ concentrations; 5-year means of these changes are shown for two different measurement programmes as thick black and thin red lines; the upper black line shows the annual increases that would have resulted if 100% of fossil fuel emissions stayed in the atmosphere. [Figure 7.3.3]

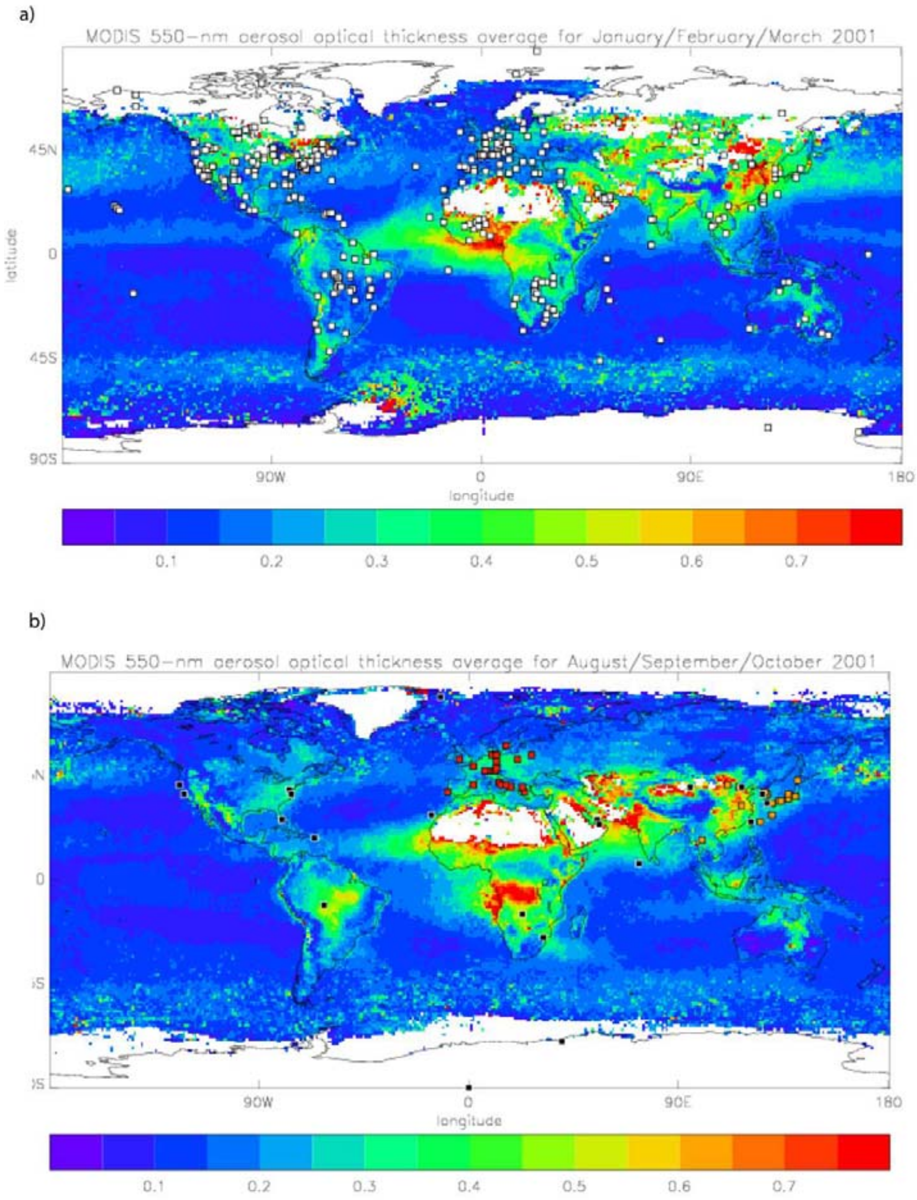


**Figure TS-4.** The total aerosol optical depth (natural plus anthropogenic) at 550 nm determined by satellite measurements for (a) January/February/March 2001 (b) for August/September/October 2001, illustrating seasonal changes in industrial and biomass burning aerosols. The locations of major international aerosols campaign studies and ground-based monitoring sites are also indicated as points. [Figure 2.13]

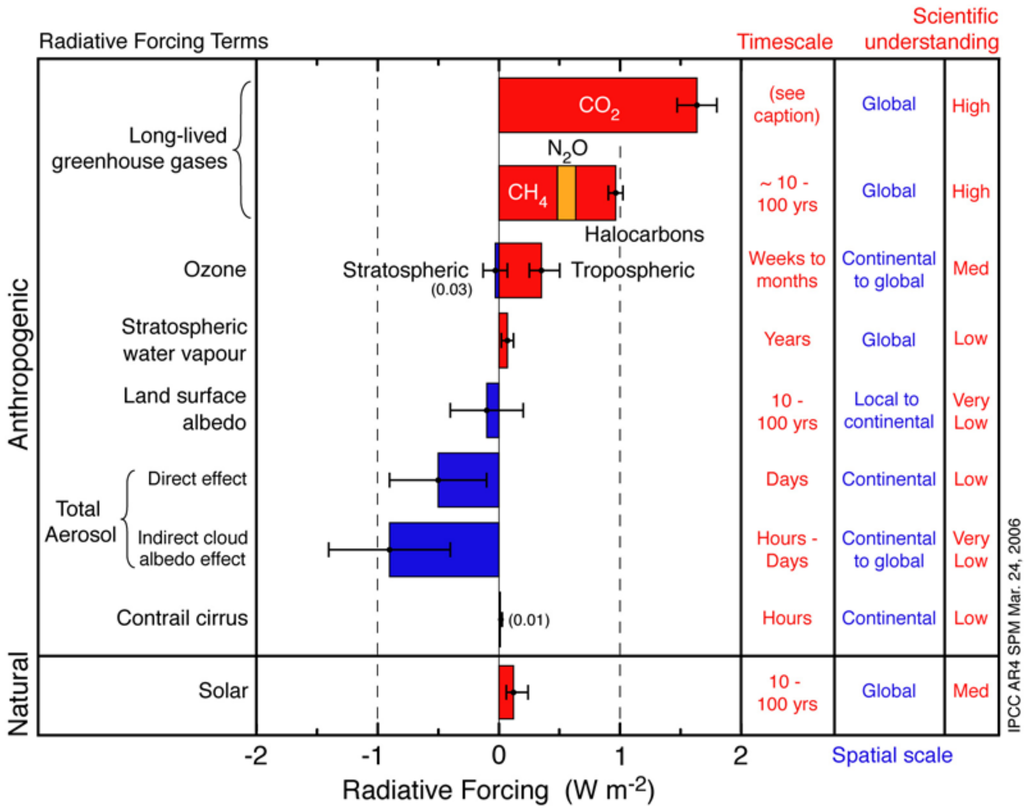


**Figure TS-5.** Global-mean radiative forcings and their 65% (1-ș uncertainty range for various agents and mechanisms. Columns on the right hand side specify: (Timescale) the approximate duration of variation/change in the agent; (Spatial scale) typical geographical extent of the forcing; (Scientific understanding) scientific confidence level as explained in Section 2.9. No $CO_2$ timescale is given as its removal from the atmosphere involves many processes and cannot be expressed accurately with a single lifetime. Errors for $CH_4$, $N_2O$, and halocarbons have been combined. [Figure 2.24]

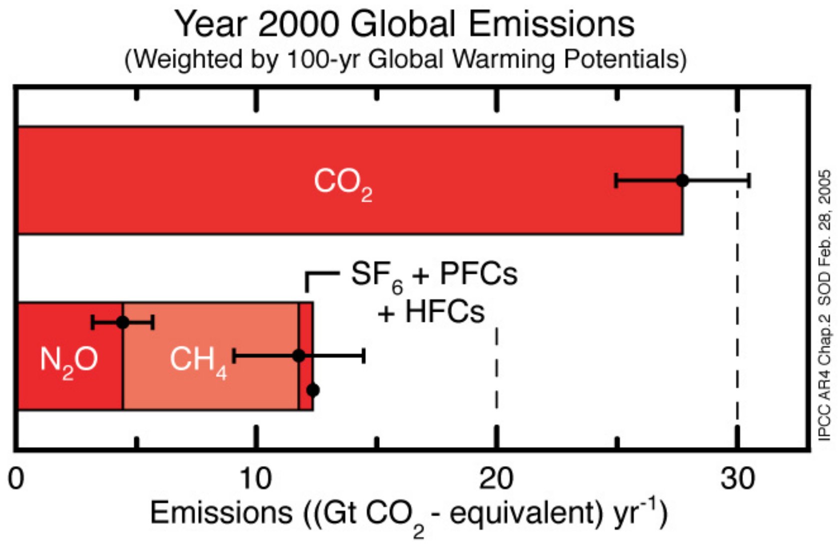


**Figure TS-6.** Estimated $CO_2$-equivalent anthropogenic emissions (i.e., emissions multiplied by 100-year GWPs) for a range of long-lived greenhouses in the year 2000 whose emissions are covered under the Kyoto Protocol. Error bars are 2-sigma and include uncertainties in both emission sources and in the GWP estimate so are larger than the uncertainties in radiative forcing for these gases which do not exceed 10%. [Figure 2.28]

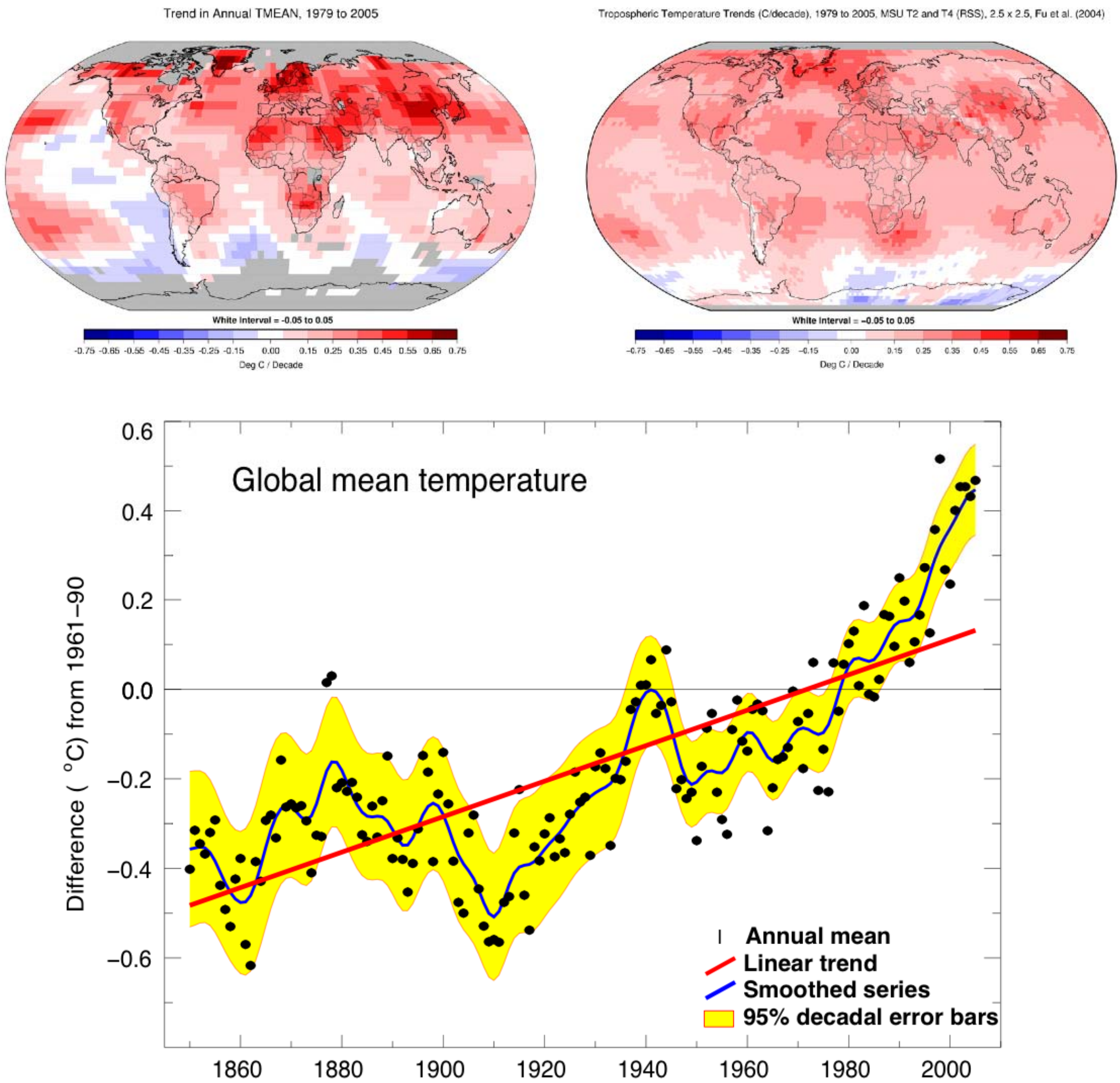


**Figure TS-7.** Top: Patterns of linear global temperature trends 1979 to 2005 estimated at the surface (left), and for the troposphere from satellite records (right). Grey areas indicate incomplete data. Bottom: The annual global mean temperatures (black dots) are given along with simple fits to the data. The red line is a linear trend fit to the complete 1850–2005 record and the blue line is a smoothed depiction to capture the decadal variations, and with decadal 95% (yellow) error range about that line. The temperature change from the first 70 years of the instrumental record (1850–1919) to the last 5 years (2001–2005) is 0.78 ± 0.18ºC. [Question 3.1, Figure 1.]

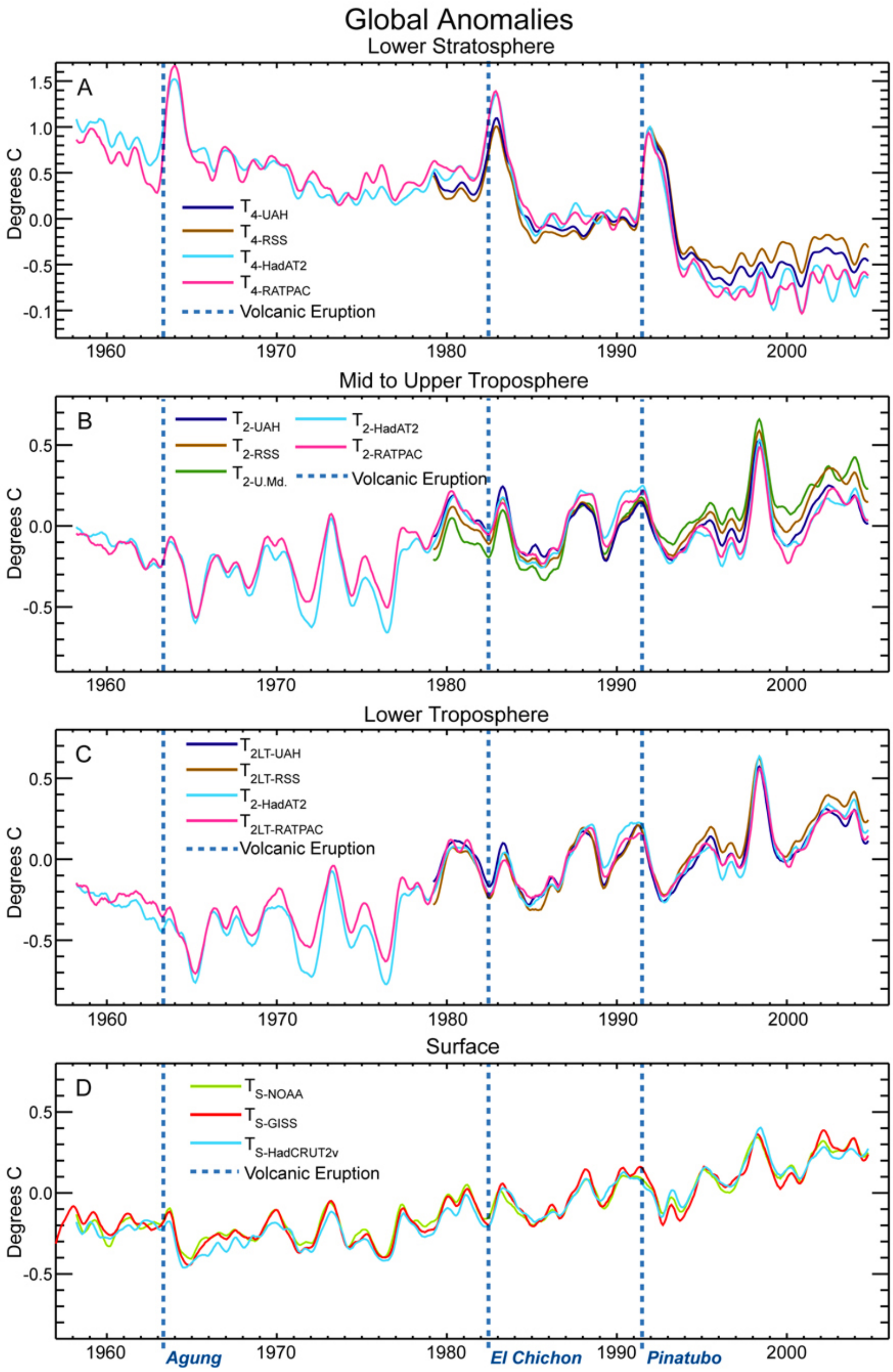


**Figure TS-8.** Observed surface and upper air temperatures (for the lower troposphere, mid to upper troposphere and lower stratosphere), as monthly mean anomalies relative to 1979–1997 smoothed with a 7-month running mean filter. Dashed lines indicate the times of major volcanic eruptions. [Figure 3.4.2]

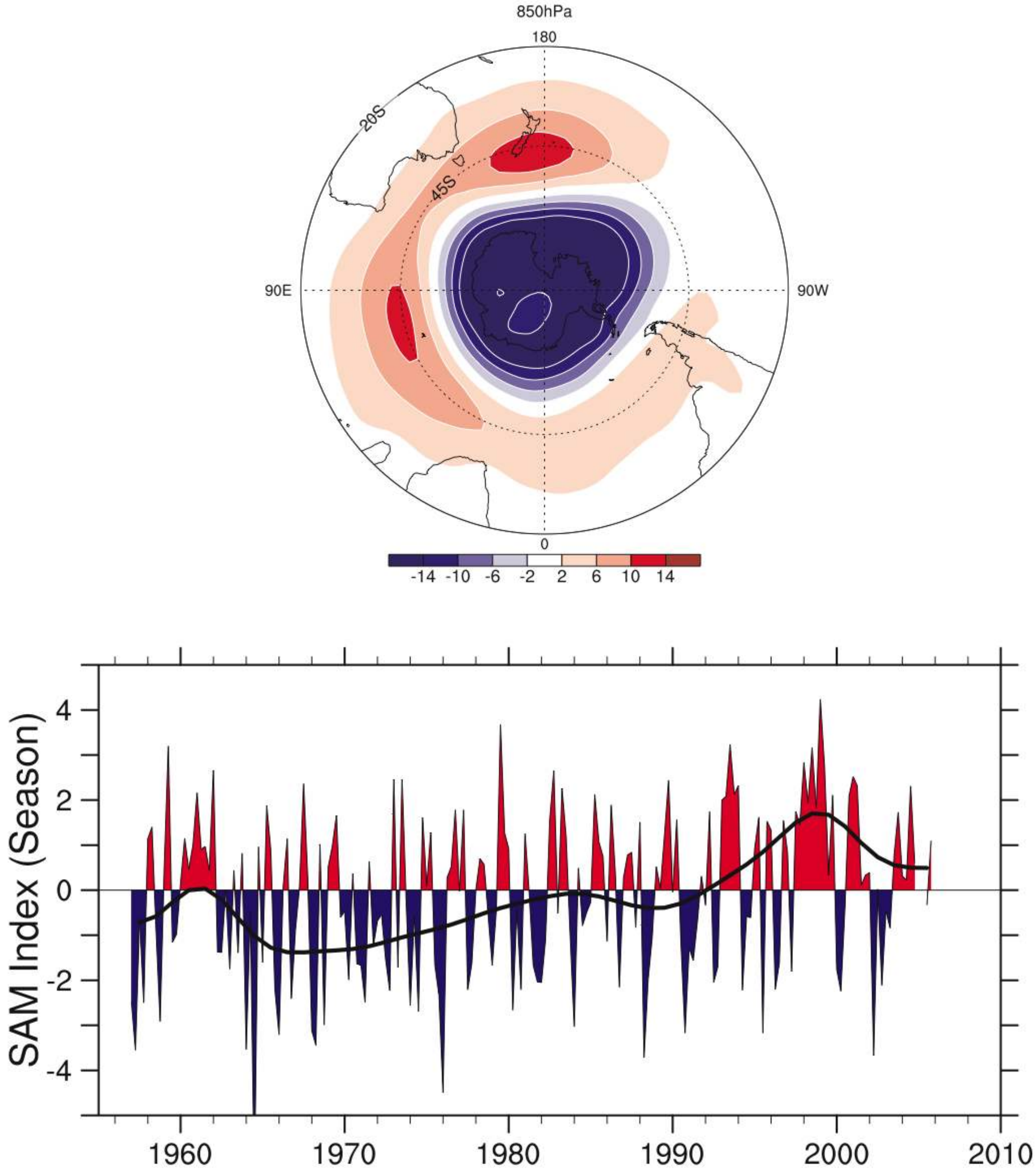


**Figure TS-9.** Top: The structure of the SAM indicated by the SAM geopotential height pattern as a regression based on the SAM time series for seasonal anomalies at 850 mbar. Bottom: Seasonal values of the Southern Annular Mode index calculated from station data. The thick black line is a decadal filter. [Figure 3.6.7]

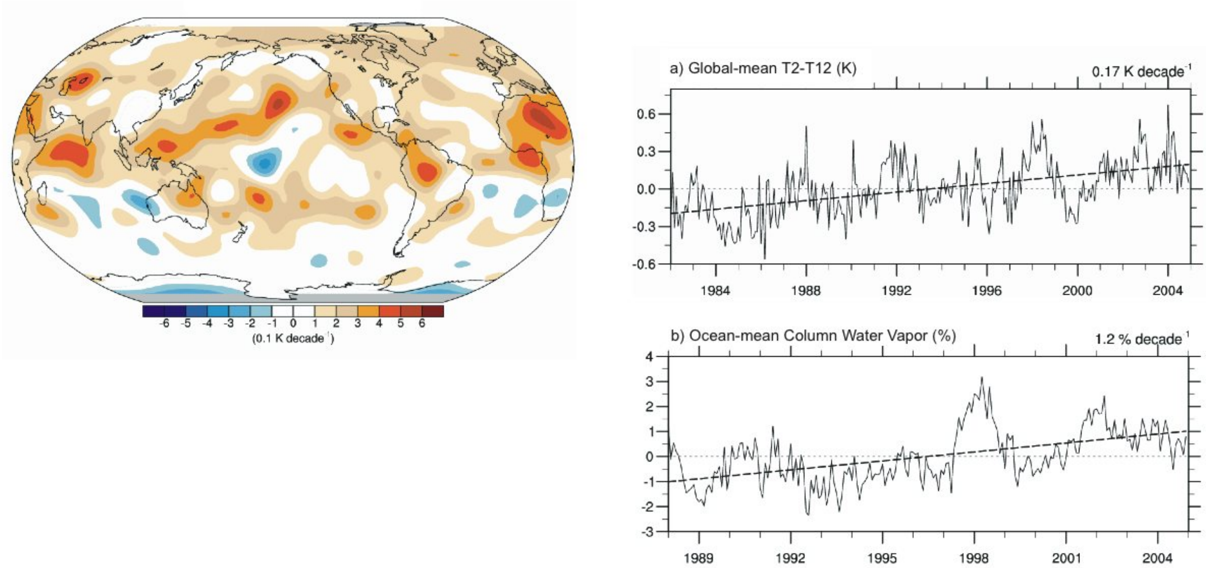


**Figure TS-10.** The radiative signature of upper tropospheric moistening is given by upward linear trends in T2–T12 for 1982–2004 shown as an anomaly map in 0.1°C per decade (top left) and monthly time series of the global-mean anomalies and linear trend (dashed) (top right) . The monthly time series of anomalies in total precipitable water over the global ocean for 1988–2004 and their linear trend are shown in the bottom panel. [Figures 3.4.5, 3.4.6]

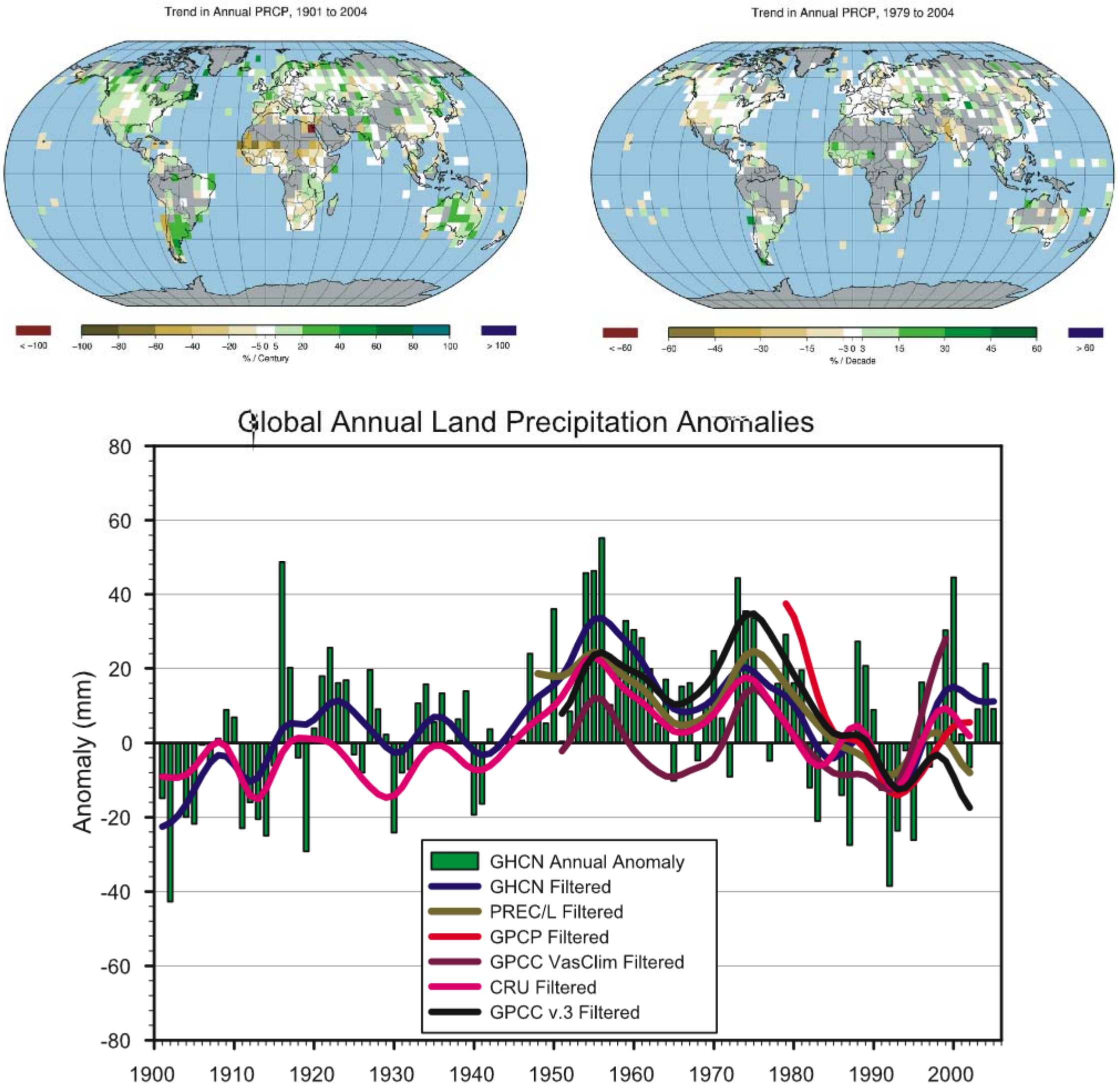


**Figure TS-11.** Top: Distribution of trends of annual precipitation amounts for 1901–2005 (left) and 1979–2004 (right). Areas in grey have insufficient data to produce reliable trends. The units are % per century and % per decade as indicated, the percentage being based on the 1961–1990 period. Bottom: Time series of annual global land precipitation anomalies with respect to the 1961–90 base period for 1900 to 2004. Smoothed values are also indicated. **[**Figure 3.3.1 and 3.3.2]

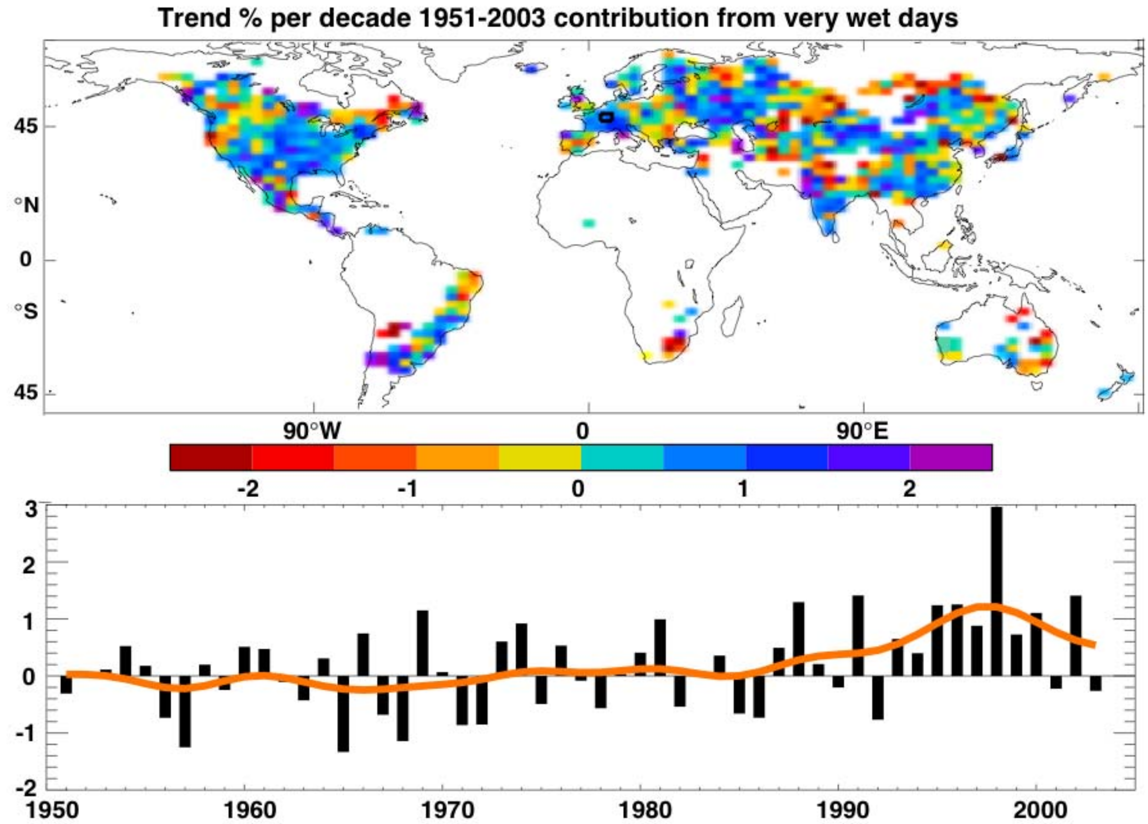


**Figure TS-12.** Upper: Observed trends (%) per decade for 1951–2003 for the contribution to total annual precipitation from very wet days corresponding to the 95th percentile. Middle: Anomalies of the global annual time series of very wet days (with respect to 1961–90) defined as the percentage change from the base period average (22.5%). The orange line shows decadal variations. Lower: Regions where disproportionate changes in heavy and very heavy precipitation during the past decades were documented compared to the change in the annual and/or seasonal precipitation. Thresholds used to define "heavy" and "very heavy" precipitation vary by season and region. [Figure 3.8.2]

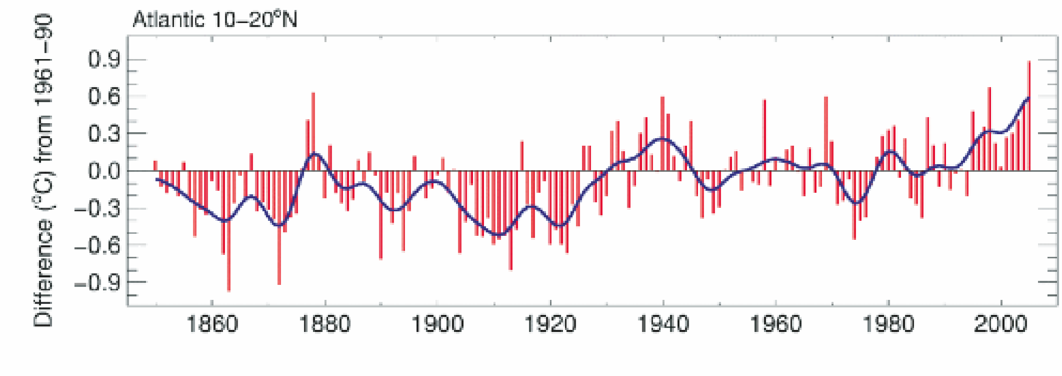


**Figure TS-13.** Tropical Atlantic (10–20°N) sea surface temperature annual anomalies in the region of Atlantic hurricane formation, relative to 1961–1990 mean (°C). [Figure 3.6.8]

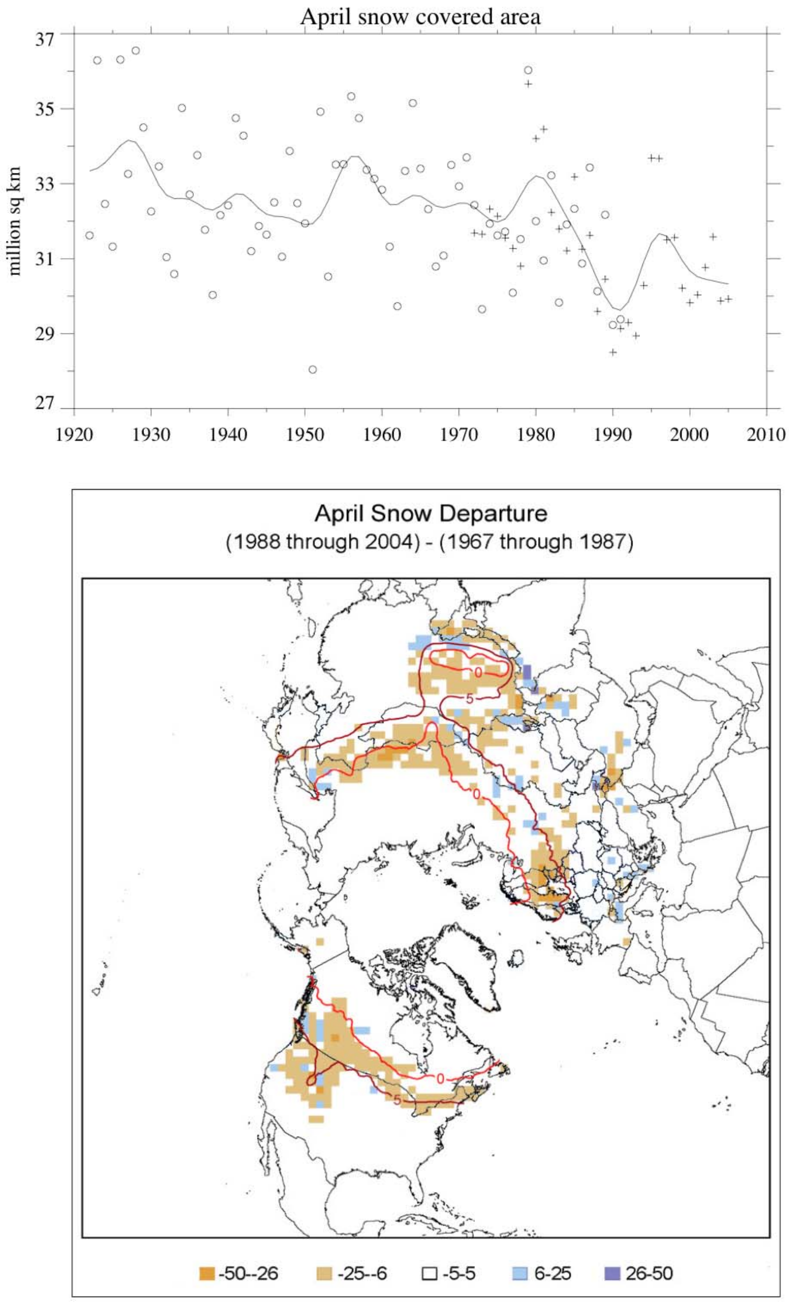


**Figure TS-14.** Top: Northern hemisphere April snow cover area. Open circles are from a station-derived snow cover index and plus symbols are from satellite data. [Figure 4.2.1.] Bottom: Differences in the distribution of April snow cover between earlier (1967–1987) and later (1988–2004) portions of the satellite era (expressed in percent coverage). Tan colours show areas where snow cover has declined. Most decline occurred between the 0°C and 5°C isotherms shown in red (for April averaged over 1967 – 2004) owing to strong temperature feedback. [Figure 4.2.2]

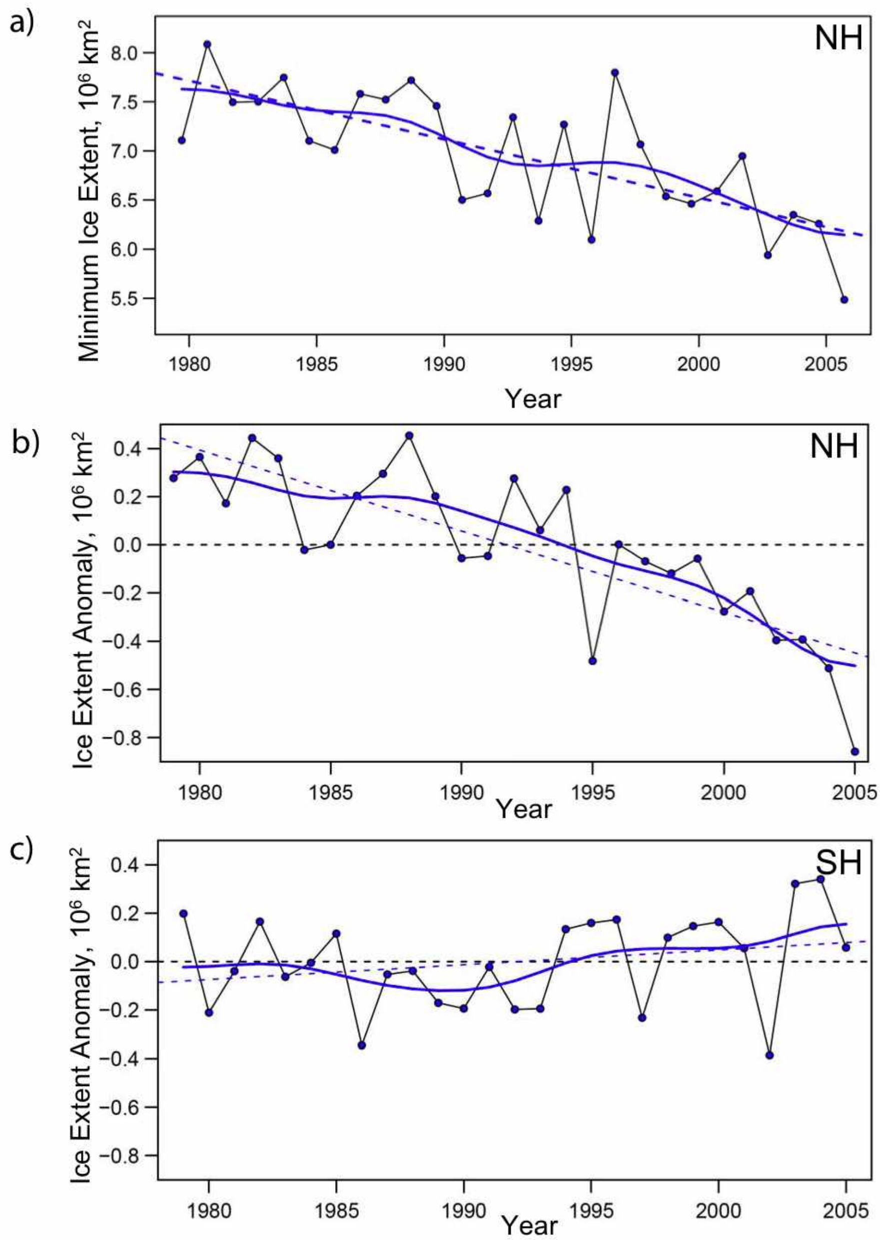


**Figure TS-15. (**a) Arctic minimum sea ice extent (1979–2005); (b) Arctic sea ice extent anomalies (1979–2005); (c) Antarctic sea ice extent anomalies (1979–2005). Symbols indicate annual mean values while the curves are the result of a 13-point time filter. The dashed lines indicate the linear trends. (a) Results show a linear trend of –60 ± 24 x $10^3$ $km^2$ year, or approximately –8% per decade. (b) The linear trend is –33 ± 8.8 x $10^3$ $km^2$ $yr^{-1}$ (equivalent to approximately –2.6% per decade) and is significant at the 95% confidence level. (c) Antarctic results show a small positive trend of 5.6 ± 11 x $10^3$ $km^2$ $year^{-1}$ which is not significant. [Figure 4.4.1 and 4.4.2]

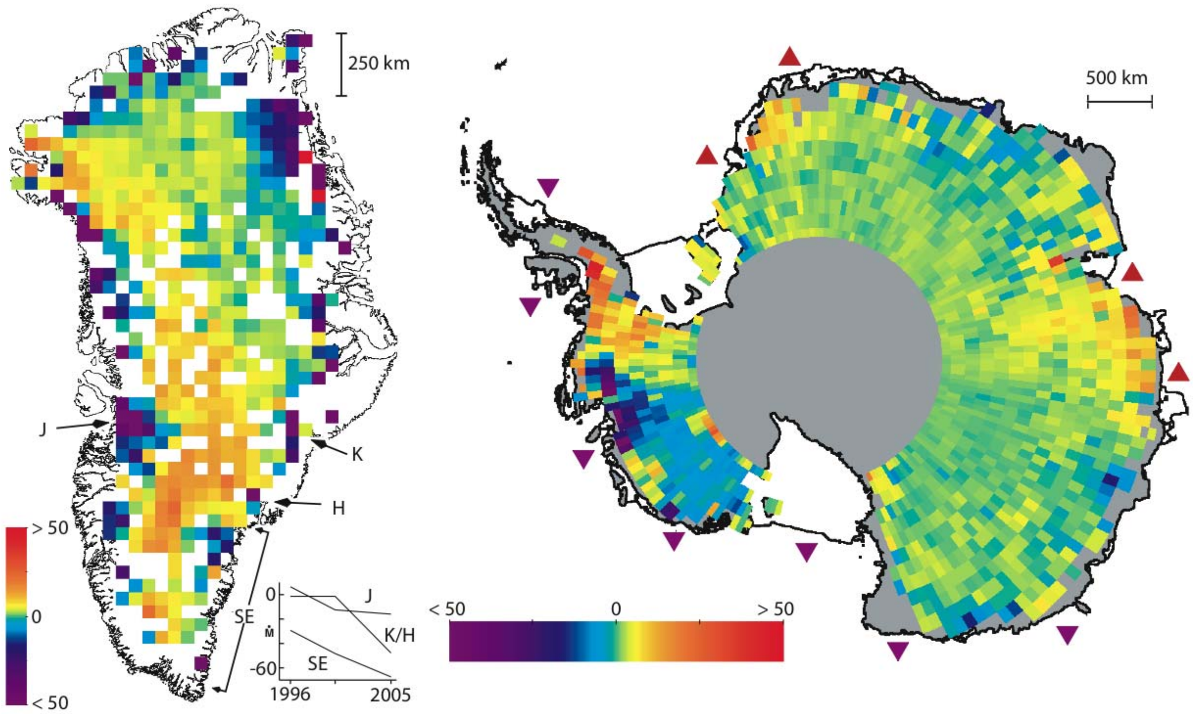


**Figure TS-16.** Rates of observed recent (1989–2005; 1992–2005) surface-elevation change for Greenland (left) and Antarctica (right), respectively. Red indicates a rising surface and blue a falling surface, which typically indicate increase or loss in ice mass at a site, although changes over time in bedrock elevation and in near-surface density can be important. For Greenland, the rapidly thinning outlet glaciers Jakobshavn (J), Kangerdlugssuaq (K), Helheim (H), and areas along the southeast coast (SE) are shown, together with their estimated mass balance versus time (with K and H combined, in Gt yr$^{-1}$, with negative values indicating loss of mass from the ice sheet to the ocean. For Antarctica, ice shelves estimated to be thickening or thinning by more than 30 cm yr$^{-1}$ are shown by point-down purple triangles (thinning) and point-up red triangles (thickening) plotted just seaward of the relevant ice shelves. [Figure 4.6.1 and 4.6.3]

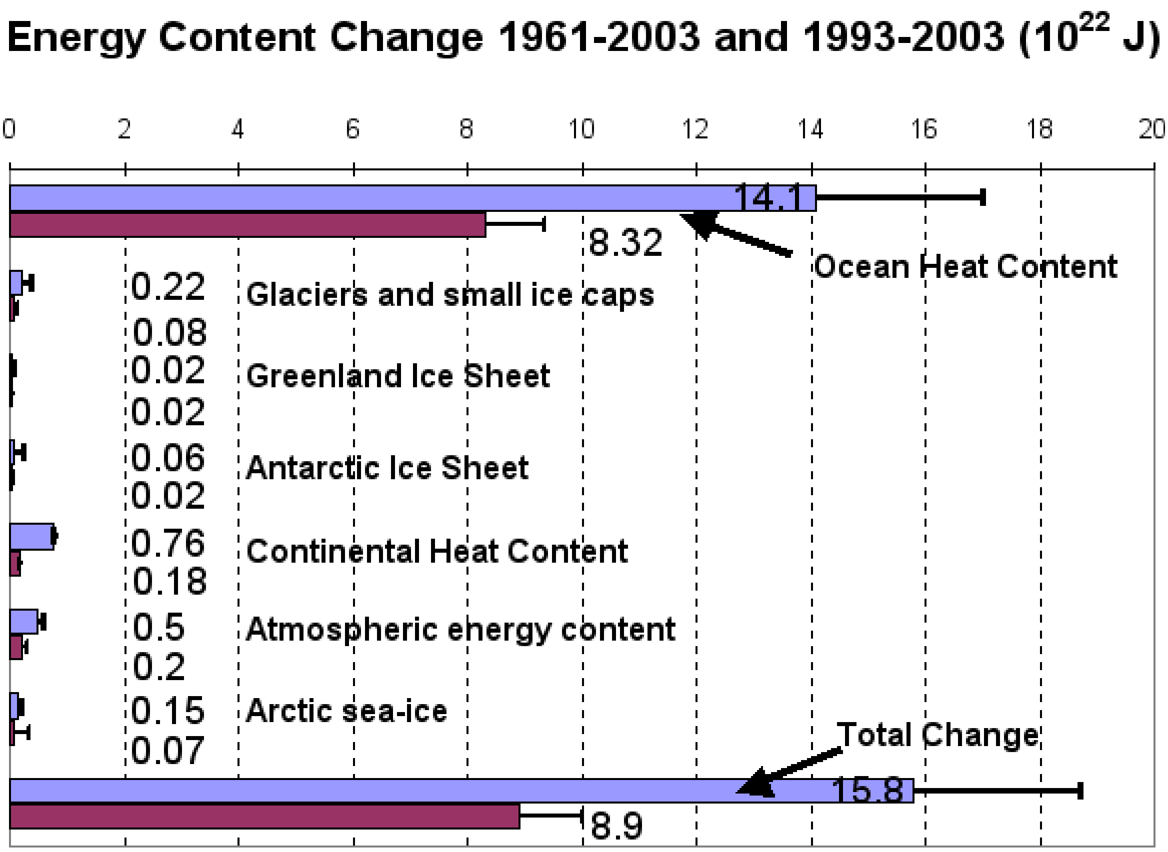


**Figure TS-17.** Energy content changes from differing components of the Earth Systems for two periods (1961–2003) and (1993–2003). Blue bars are for 1961–2003; burgundy bars are for 1993–2003. Positive energy content change means an increase in stored energy (or heat in oceans). All error estimates are 95% confidence intervals. No estimate of confidence is available for the continental heat gain. Some of the results have been scaled from published results for the two respective periods. **[**Figure 5.2.5]

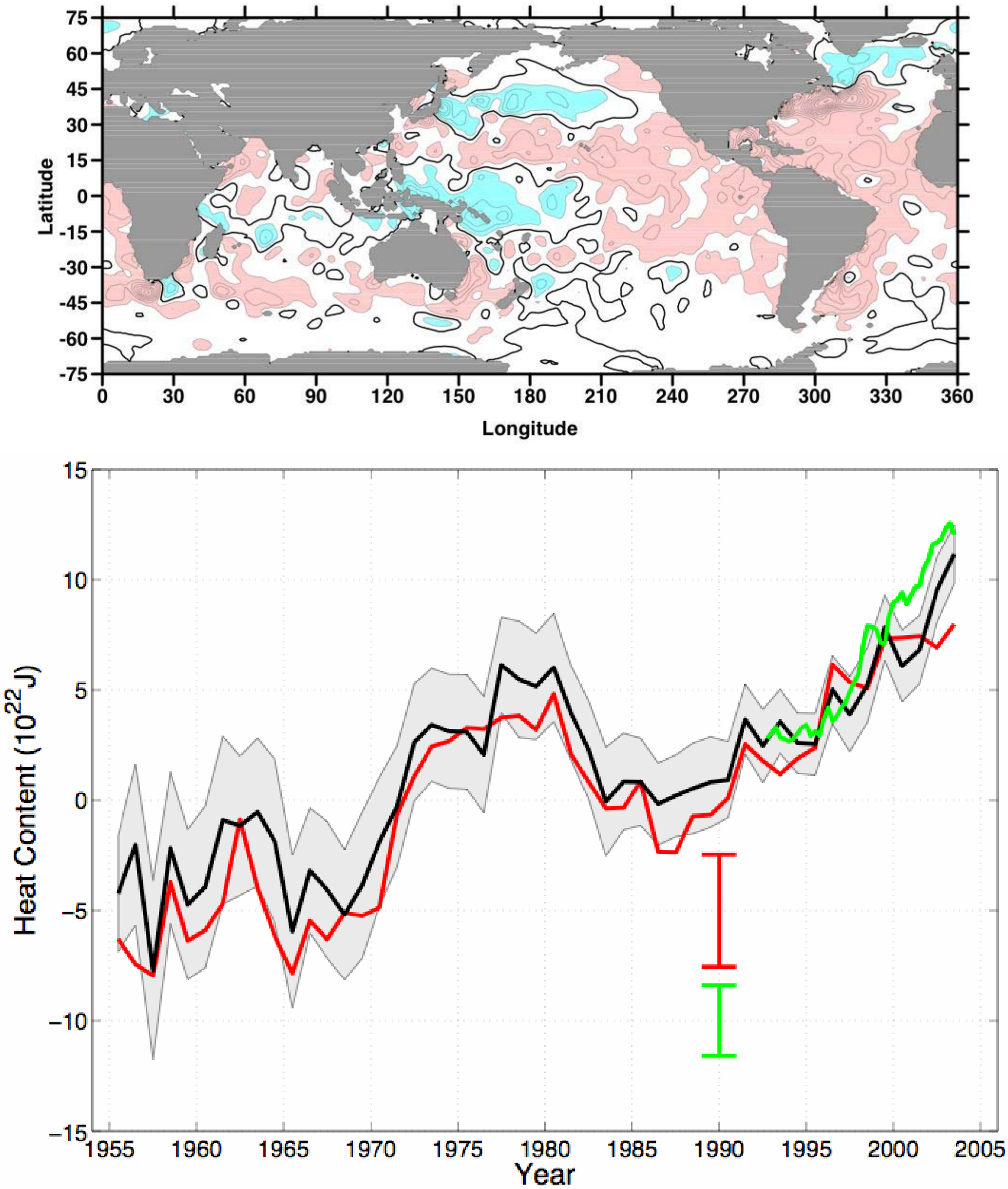


**Figure TS-18.** Top: Linear trends in ocean heat content for the 0–700 m layer over the 1955–2003 period with a contour interval of 1 x $10^{17}$ J $yr^{-1}$. [Figure 5.2.1] Bottom: Time series of yearly ocean heat content ($10^{22}$ J) for the 0–700 m layer. Different colours indicate three different analyses of the data. The 95% uncertainty range for the black curve is indicated by the grey curves and for the other two curves by the error bars [Figure 5.2.2].

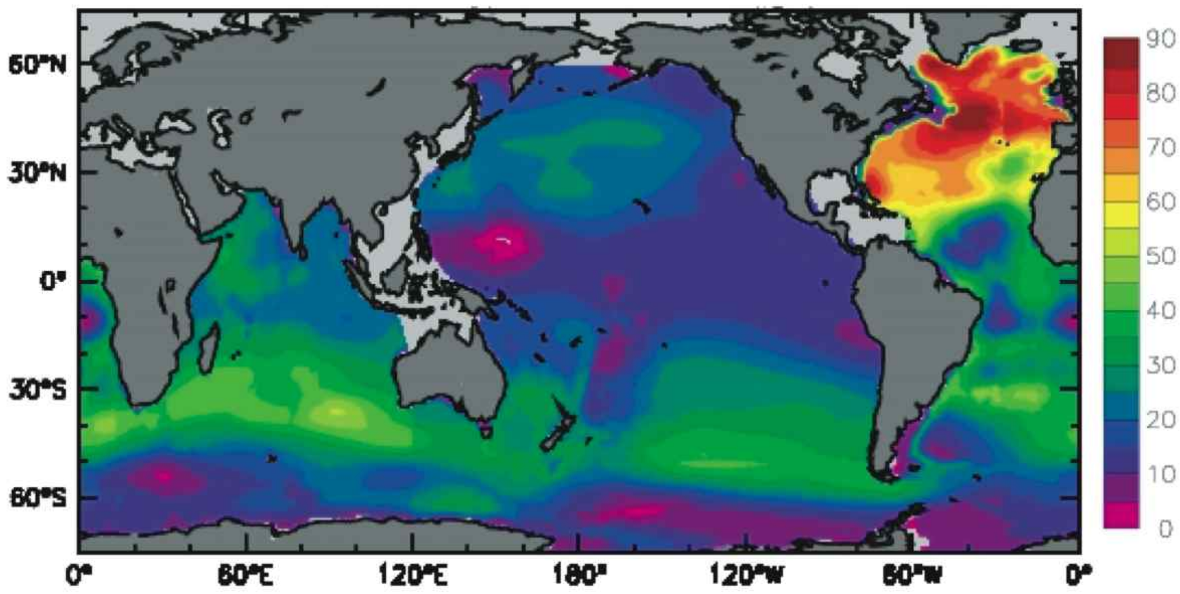


**Figure TS-19.** Inventory of anthropogenic carbon (mol/m$^2$) for the year 1994. Anthropogenic carbon is estimated indirectly by correcting measured dissolved inorganic carbon (DIC) for the contributions of organic matter decomposition and dissolution of carbonate minerals, and taking into account the DIC concentration the water had in the pre-industrial ocean when it was last in contact with the atmosphere. The global inventory of anthropogenic carbon taken up by the ocean between 1750 and 1994 is estimated to be 118 ± 19 GtC. [Figure 5.4.2**]**

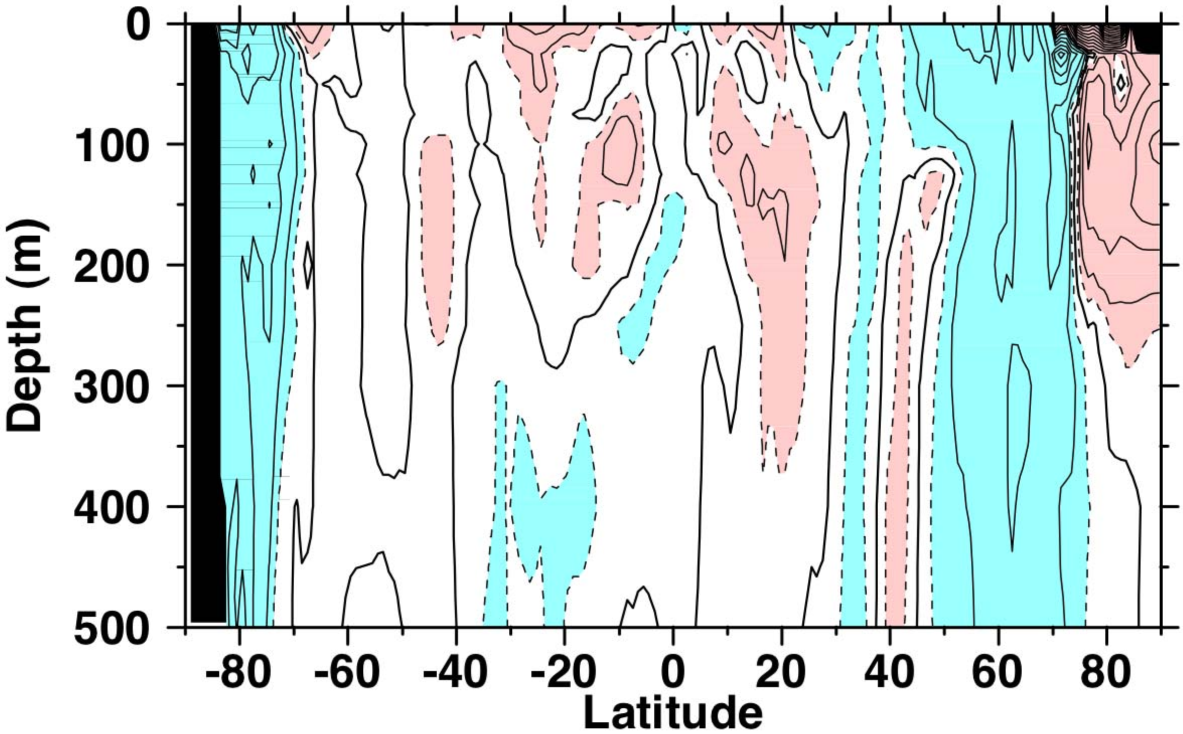


**Figure TS-20.** Linear trend (1955–1998) of zonally averaged salinity for the World Ocean. Contour interval is 0.01 per decade and dashed contours are ±0.005 per decade. Dark, solid line is the zero contour. Red shading indicates values equal or greater than 0.005 decade$^{-1}$ and blue shading indicates values equal or less than –0.005 per decade. [Figure 5.2.6]

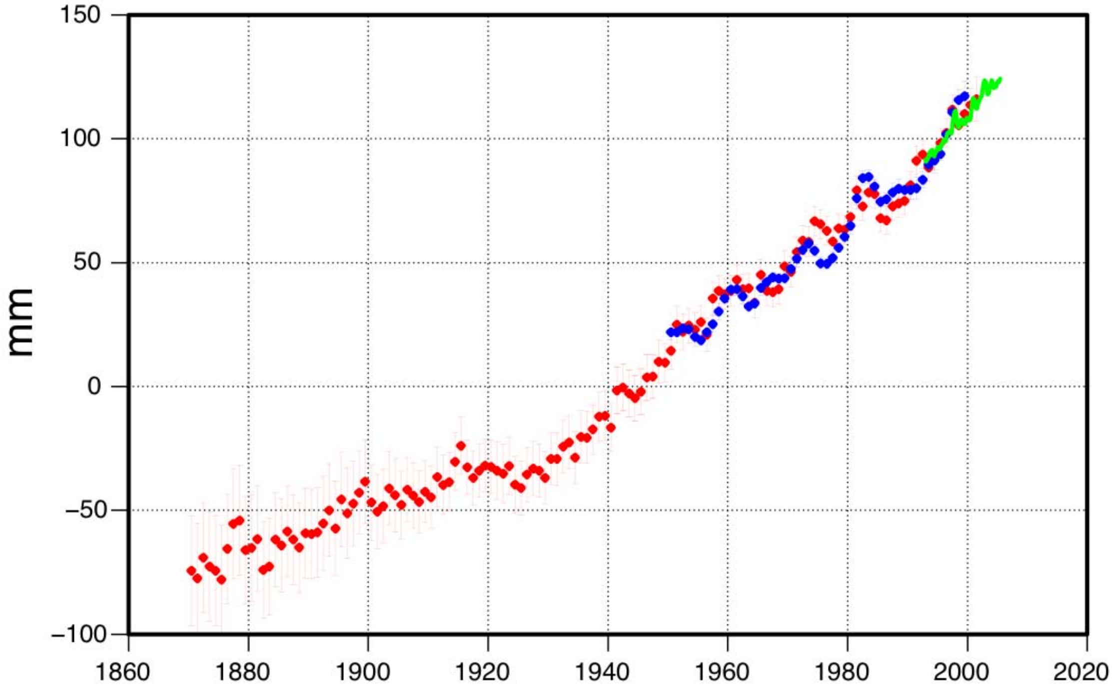


**Figure TS-21.** Annual averages of the global mean sea level based on the reconstructed sea level fields since 1870 (red), tide gauge measurements (blue) since 1950, and satellite altimetry (green) since 1992. Units are in mm. **[**Figure 5.5.1]